ELSEVIER

Nuclear Instruments and Methods in Physics Research B 155 (1999) 102–109

NIM B
Beam Interactions with Materials & Atoms

www.elsevier.nl/locate/nimb

Attenuation curves in concrete for neutrons produced by 710 MeV α-particles on steel and water and by 337–390 MeV/u Ne ions on Al, Cu and Pb

S. Agosteo [a,b,*], A. Fassò [c], A. Ferrari [d,1], P.R. Sala [d,1], M. Silari [e], P. Tabarelli de Fatis [f]

[a] *Politecnico di Milano, Dipartimento di Ingegneria Nucleare, via Ponzio 34/3, 20133 Milano, Italy*
[b] *INFN Sezione di Milano, Milano, Italy*
[c] *Stanford Linear Accelerator Center, MS 48, P.O. Box 4349, Stanford, CA 94309, USA*
[d] *Istituto Nazionale di Fisica Nucleare, Sezione di Milano, via Celoria 16, 20133 Milano, Italy*
[e] *CERN, 1211 Geneva 23, Switzerland*
[f] *Fondazione TERA, via Puccini 11, 28100 Novara, Italy*

Received 2 February 1999; received in revised form 3 May 1999

Abstract

The attenuation in ordinary concrete of the total dose equivalent due to neutrons produced by 710 MeV α-particles on steel and water and by 337–390 MeV/u Ne ions on Al, Cu and Pb was calculated with the FLUKA Monte Carlo code. Experimental data (taken from the literature) of the neutron double differential distributions were utilized for the source in the calculations. The contribution of all secondaries (neutrons, photons and protons) produced in the concrete shield was considered. Source terms and attenuation lengths are given as a function of energy and emission angle.

PACS: 28.41.Q
Keywords: Ion accelerator; Shielding; Dose equivalent; Attenuation length; Source term

1. Introduction

Most light-ion accelerator laboratories are being employed for nuclear research [1], but light ions beams with energies up to several hundreds of MeV/u are also of interest in cancer therapy for both their physical and biological properties [2,3]. More than one thousand patients were treated from 1975 to 1992 at the Lawrence Berkeley Laboratory (LBL, USA) mainly with He and Ne ions [4]. A hospital-based facility for light ion treatment has started operation in 1994 in Chiba, Japan [5], a second one is under construction in Japan, in the Hyogo prefecture. Ion therapy with carbon ions just started at GSI (Darmstadt,

* Corresponding author. Tel.: +39-2-2399-6318; fax: +39-2-2399-6309; e-mail: stefano.agosteo@polimi.it
[1] Present address: CERN, 1211 Geneva 23, Switzerland.

0168-583X/99/$ – see front matter
PII: S0168-583X(99)00460-7

Germany) [6] in view of the construction of a clinical unit. Cancer treatment with light ions up to $^{12}C^{6+}$with energies up to 400 MeV/u is envisaged at the National Centre for Oncological Hadrontherapy proposed for Italy [7,8].

Secondary neutrons produced by ion interactions with the structural materials of the accelerator, of the beam transfer lines and of the beam delivery system and, in the case of medical facilities, with the patient, rule the shielding requirements of these facilities. In fact, secondary charged particles generated in the same interactions can be easily shielded locally or are stopped completely in air and/or at low depths in the concrete walls. The present work is a follow-up of Ref. [9], where attenuation curves in concrete for secondary neutrons produced by intermediate energy protons stopped in various materials were calculated. This paper presents attenuation curves of total dose equivalent (source terms and attenuation lengths) in ordinary concrete for neutrons produced by 710 MeV α-particles on steel and water targets and by 337–390 MeV/u Ne ions on aluminium, copper and lead targets. The contribution to dose equivalent of secondary protons and photons is also given. A comparison is made with proton data.

2. Neutron sources

The literature treating ion accelerator shielding is scarce and Monte Carlo codes performing ion transport with secondary particle production are lacking because the yield systematics for different combinations of bombarding ion and target is not yet supported by a sufficient set of measurements [10–12]. This subject is exhaustively discussed in Ref. [11], where is pointed out that only a limited number of measurements of thick-target neutron yields (TTNY) for α-particles are available, while no experimental data on differential TTNY existed for heavier particles before that work was published. Several combinations of target and projectiles were considered in the measurements discussed in Ref. [11] at energies of about 10 MeV/u, which are below the range of interest for the present work. At higher energies, which are of interest for cancer therapy, differential cross sections of neutron production were measured for specific combinations of projectile and targets [13–15]. New experimental data on angular and energy distributions of neutrons produced by light ions in the energy range 100–400 MeV/u were recently published [16], soon after the present work was completed.

The attenuation through ordinary concrete of the dose equivalent due to neutrons produced by ion interactions in some materials of interest can be calculated by utilizing either the available experimental TTNY double distributions or parametric expressions based on the existing nuclear models, as the source of an appropriate Monte Carlo code. Although a few models for secondary particle production following ion interactions can be found in the literature [10,11,17–23], experimental data were used in the present work because, as mentioned above, measurements supporting the validity of these parametric expressions are still scarce.

Different source neutrons were used in the present work:

1. Neutrons produced by 710 MeV α-particles completely stopping in steel (target thickness 4.445 cm) and water (target thickness 22.86 cm) [15]. Steel is a typical structural material of accelerators and beam lines, while water can simulate the patient.
2. Neutrons produced by 337 MeV/u neon ions on aluminum and copper [13], where the target thickness was such that only about 20% of the beam energy was lost.
3. The differential neutron production cross sections of 390 MeV/u Ne ions on a thin (0.3 cm) lead target [14]. Lead is the typical material used as a scatterer in the beam delivery system to increase the irradiation field.

The neutron spectra at 0° from 710 MeV (177.5 MeV/u) α-particles striking a steel and a water target are compared with those generated by 150 MeV protons on iron and soft tissue [9] in Figs. 1 and 2. A larger high energy component can be observed in both figures for neutron spectra produced by α-particles.

The attenuation in concrete was calculated with the FLUKA Monte Carlo code [24–29] at the angles where experimental data were available

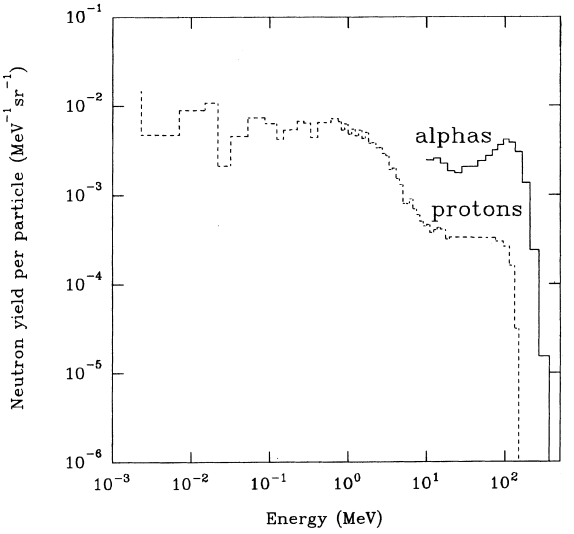

Fig. 1. Energy distribution of neutrons produced at 0° for 710 MeV α-particles striking a thick steel target (experimental [14]) and 150 MeV protons on iron (calculated [8]).

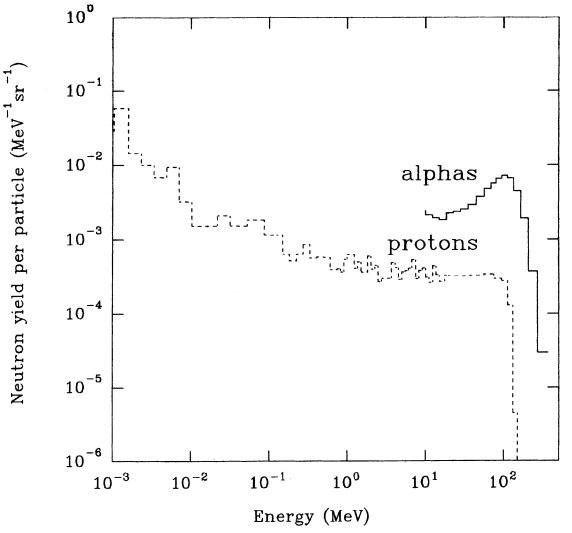

Fig. 2. Energy distribution of neutrons produced at 0° for 710 MeV α-particles striking a thick water target (experimental [14]) and 150 MeV protons on soft-tissue (calculated [8]).

[13–15], i.e., from 0° to 140° for 710 MeV α-particles and 390 MeV/u Ne ions on lead and from 30° to 90° for 337 MeV/u Ne ions on aluminum and copper.

The FLUKA code transports hadrons, leptons and photons from thermal energies up to several TeV and treats both hadronic and electromagnetic showers. In the intermediate energy range (below a few GeV up to a few tens MeV) secondary hadron production is performed with the intranuclear cascade model, followed by pre-equilibrium emission, nuclear evaporation/fragmentation and residual nucleus deexcitation with photon emission. Neutron transport below 19.6 MeV is ruled by discrete cross sections subdivided into 72 energy groups.

The results of the calculations were fitted by the classical two-parameter formula (Section 4). The contribution of both neutrons and their secondaries produced in the concrete were taken into account.

3. Neutron attenuation in concrete

The neutron attenuation in concrete type TSF 5.5 [30] was computed with FLUKA for concrete thickness from 0 to 600 cm. The simulation geometry and characteristics are the same utilized in previous calculations for protons impinging on targets of various materials [9] and are briefly recalled here.

A point neutron source with the double differential distributions taken from Refs. [13–15] was placed at the centre of a sphere whose inner radius was large enough to ensure that effects related to curvature are negligible. A comparison between spherical and slab geometry showed that the results agree within the statistical uncertainties [9]. The computed particle fluence was scored with cosine weighted boundary crossing estimators for various concrete shells of different thickness (steps of 10 cm from 0 to 40 cm, 20 cm from 40 to 200 cm and 40 cm from 200 to 600 cm). In particular, each shell was considered in a separate simulation. This procedure, although very time consuming, was preferred to that calculating the fluence on fictitious surfaces placed at different depths of a bulky shield. The method adopted in the present work eliminates the risk of overestimating the fluence of neutrons and prompt gamma rays due to neutron reflection in the remainder of the shield behind the scoring surface.

The dose equivalent was calculated by folding the fluence with appropriate fluence to ambient dose equivalent conversion coefficients. The ambient dose equivalent of neutrons above and below 20 MeV was calculated with the conversion coefficients of Ref. [31]. Conversion coefficients for secondary photons and protons were taken from Refs. [31,32], respectively.

"Geometry splitting" and "Russian roulette" were employed as variance reduction techniques, adjusting the importances so as to maintain the number of particles approximately constant with increasing concrete thickness. The uncertainties on total dose equivalent values were within 5%.

4. Shielding parameters

The contribution of photons to total dose equivalent is relevant both in the case of neutrons produced by α-particles and Ne ions, while that of protons is negligible (excluding the case of Ne ions on a thin lead target). Tables 1 and 2 list the maximum percentage contributions to total dose equivalent of photons and protons for some of the projectile and target combinations investigated. The photon contribution to dose equivalent tends to increase with the emission angle, i.e., with decreasing average energy of the spectrum.

Table 1
Maximum percentage contribution to total dose equivalent of protons (p) and photons (γ) for a steel target bombarded by 710 MeV α particles

Angular bin	H_γ/H_{tot} (%)	H_p/H_{tot} (%)
Steel		
0°–10°	28.0	1.7
10°–20°	29.6	1.6
20°–30°	30.9	1.1
30°–40°	32.2	<1.0
40°–50°	30.5	<1.0
50°–60°	32.5	<1.0
60°–70°	31.3	<1.0
70°–80°	31.9	<1.0
80°–90°	28.3	0.1
90°–100°	32.2	0.1
100°–110°	28.1	<0.1
110°–120°	31.4	<0.1
120°–130°	31.5	<0.1
130°–140°	33.2	<0.1

Table 2
Maximum percentage contribution to total dose equivalent of protons (p) and photons (γ) for aluminum and copper targets bombarded by 337 MeV/u Ne ions

Angular bin	H_γ/H_{tot} (%)	H_p/H_{tot} (%)
Aluminum		
30°–40°	29.0	2.0
40°–50°	29.5	1.7
50°–60°	29.8	1.4
60°–70°	30.5	1.0
70°–80°	31.8	0.7
80°–90°	33.2	0.5
Copper		
30°–40°	27.0	1.9
40°–50°	27.2	1.6
50°–60°	28.1	1.2
60°–70°	28.4	0.9
70°–80°	29.2	0.6
80°–90°	30.5	0.5

The values of the calculated total dose equivalent can be fitted with an exponential function

$$H(E_p,\theta,d/\lambda_\theta)=\frac{H_0(E_p,\theta)}{r^2}\exp\left[-\frac{d}{\lambda_\theta g(\theta)}\right],$$

where H is the dose equivalent beyond the shield, H_0 is the source term along the direction θ with respect to the beam, r the distance between the radiation source (the target on which the ions impinge) and the point where the dose equivalent is scored, d the shielding thickness and λ_θ the attenuation length in the material in the direction θ. The function $g(\theta)$ is defined as

$$g(\theta)=\begin{cases}\cos\theta, & \text{for forward shielding,}\\ \sin\theta, & \text{for lateral shielding,}\\ 1, & \text{for the spherical geometry used in the present calculations.}\end{cases}$$

H_0 and λ are assumed to be geometry independent [9]. The source terms H_0 per primary particle (Sv m^2) and the attenuation lengths λ (g cm^{-2}) are given in Tables 3 and 4 for the various ions and targets. The deviations of the FLUKA results from the best fit are within 15% in all cases. The attenuation lengths were obtained by fitting the data beyond 1 m thickness where the

Table 3
Source term and attenuation length in concrete TSF 5.5 for total dose equivalent from steel and water targets bombarded by 710 MeV α particles

Angular bin	H_0 (Sv m^2 particle^{-1})	λ (g cm^{-2})
Steel		
0°–10°	4.02×10^{-16}	133.0
10°–20°	3.69×10^{-16}	132.1
20°–30°	2.58×10^{-16}	126.3
30°–40°	1.31×10^{-16}	120.4
40°–50°	2.46×10^{-17}	113.0
50°–60°	1.14×10^{-17}	108.6
60°–70°	8.43×10^{-18}	104.7
70°–80°	6.12×10^{-18}	100.2
80°–90°	3.58×10^{-18}	95.1
90°–100°	1.70×10^{-18}	92.2
100°–110°	8.40×10^{-19}	86.3
110°–120°	6.59×10^{-19}	80.4
120°–130°	4.48×10^{-19}	75.1
130°–140°	2.91×10^{-19}	69.5
Water		
0°–10°	9.83×10^{-16}	136.3
10°–20°	5.93×10^{-16}	134.2
20°–30°	2.10×10^{-16}	125.5
30°–40°	9.69×10^{-17}	122.4
40°–50°	5.86×10^{-17}	115.7
50°–60°	3.81×10^{-17}	110.5
60°–70°	2.61×10^{-17}	106.1
70°–80°	1.60×10^{-17}	101.6
80°–90°	1.17×10^{-17}	92.7
90°–100°	7.09×10^{-18}	88.8
100°–110°	4.74×10^{-18}	85.1
110°–120°	3.98×10^{-18}	77.4
120°–130°	3.46×10^{-18}	70.6
130°–140°	2.99×10^{-18}	65.3

Table 4
Source term and attenuation length in concrete TSF 5.5 for total dose equivalent from aluminium and copper targets bombarded by 337 MeV/u Ne ions and a lead target bombarded by 390 MeV/u Ne ions

Angular bin	H_0 (Sv m^2 particle^{-1})	λ (g cm^{-2})
Aluminium		
30°–40°	3.31×10^{-17}	132.6
40°–50°	1.83×10^{-17}	127.7
50°–60°	1.10×10^{-17}	123.8
60°–70°	6.38×10^{-18}	118.3
70°–80°	3.45×10^{-18}	112.1
80°–90°	2.33×10^{-18}	101.3
Copper		
30°–40°	3.29×10^{-17}	131.6
40°–50°	1.95×10^{-17}	126.3
50°–60°	1.20×10^{-17}	117.5
60°–70°	7.99×10^{-18}	110.3
70°–80°	5.42×10^{-18}	103.8
80°–90°	3.42×10^{-18}	98.5
Lead		
0°–10°	6.36×10^{-15}	137.3
10°–20°	1.51×10^{-15}	190.1
20°–30°	4.89×10^{-16}	180.8
30°–40°	3.02×10^{-16}	173.8
40°–50°	2.20×10^{-16}	171.8
50°–60°	6.81×10^{-17}	156.4
60°–70°	5.05×10^{-17}	147.0
70°–80°	4.34×10^{-17}	140.6
80°–90°	3.25×10^{-17}	134.1
90°–100°	2.88×10^{-17}	127.4
100°–110°	2.09×10^{-17}	116.5
110°–120°	1.88×10^{-17}	107.4
120°–130°	1.57×10^{-17}	96.5
130°–140°	1.43×10^{-17}	89.0

transmission curves are roughly exponential, showing that the neutron spectrum has reached equilibrium in the concrete. The behavior of H_0 and λ as a function of the minimum shielding thickness included in the fit is thoroughly discussed in Ref. [9].

Figs. 3–5 show the transmission curves for the various ion and target combinations taken into account. At small depths and small angles a dose build-up region is visible in all cases. Moving towards larger angles, particularly for thick targets, this situation is reversed and a fast attenuation region appears at small thickness, due to the rapid attenuation of the soft component of the spectrum. The attenuation curves at 0° for neutrons from 150 MeV protons on iron and tissue [9] are compared in Fig. 6 with those for 710 MeV (177.5 MeV/u) α-particles on steel and water. This comparison has significance as the energy per nucleon is about the same. The attenuation is smaller in the case of α-particles, which produce neutron energy distributions with a much larger high energy component, as shown in Figs. 1 and 2.

Figs. 7 and 8 show the attenuation lengths and the source terms vs. the scoring angle θ. A rather smooth behavior can be observed in all cases.

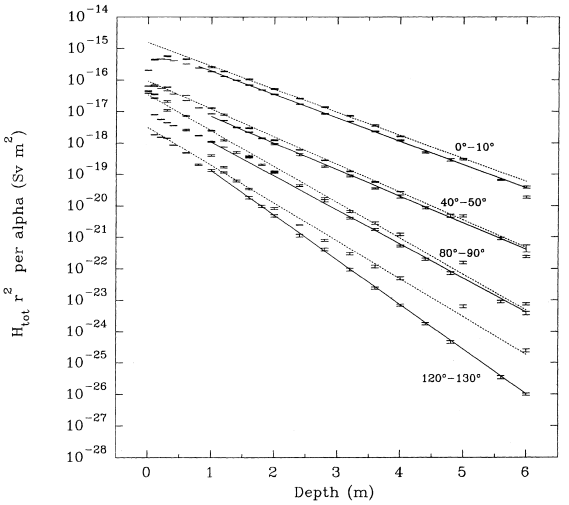

Fig. 3. Attenuation of total dose equivalent in ordinary concrete for 710 MeV α-particles striking a thick water (solid line) and a steel (dashed line) target.

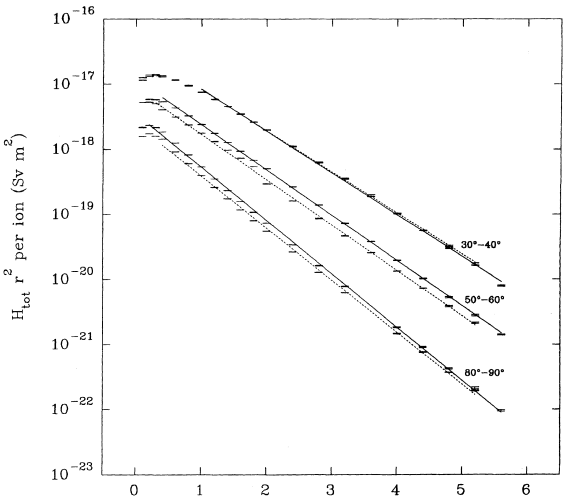

Fig. 4. Attenuation of total dose equivalent in ordinary concrete for 337 MeV/u Ne ions striking a thin copper (solid line) and a aluminum (dashed line) target.

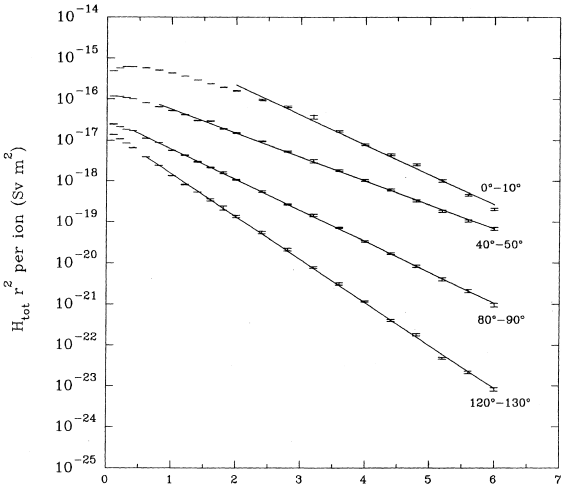

Fig. 5. Attenuation of total dose equivalent in ordinary concrete for 390 MeV/u Ne ions striking a thin lead target.

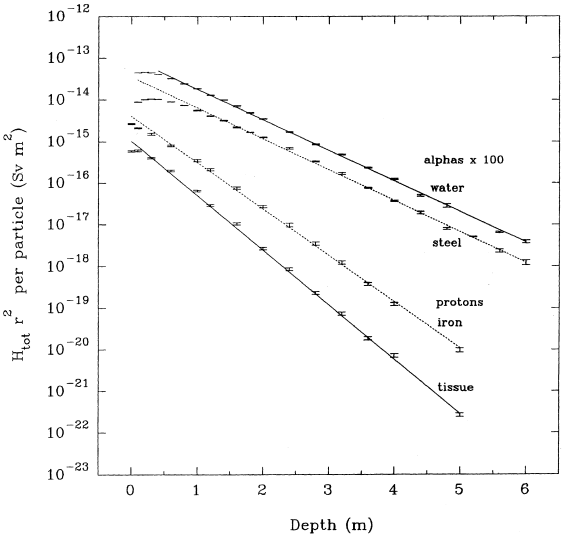

Fig. 6. Attenuation of total dose equivalent in ordinary concrete in the interval 0°–10° for 710 MeV α-particles striking thick steel and water targets and for 150 MeV protons on iron and soft-tissue [8].

5. Discussion and conclusions

The results of the present work are intended to be of some help for the shielding design of ion-accelerator facilities, for some ion-target combinations. Due to the lack of reliable nuclear models allowing Monte Carlo calculations and of a comprehensive set of experimental data, the present data may be also useful for other cases.

It should be pointed out that the attenuation curves for Ne ions on Al, Cu and Pb should not be used for shielding calculations of losses in which

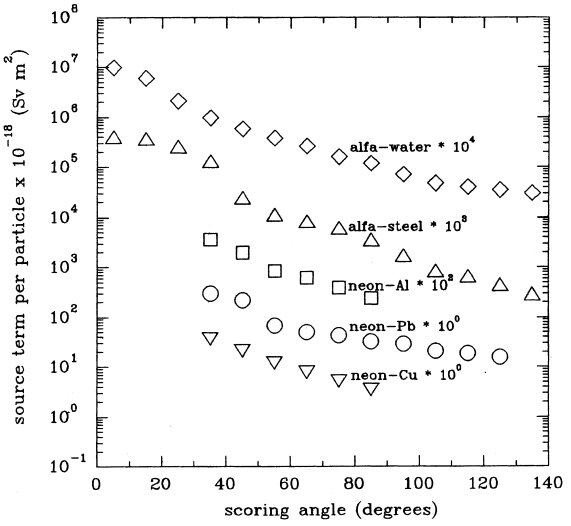

Fig. 7. Source term H_0 (Sv m^2 particle^{-1}) versus scoring angle θ for various projectile–target combinations.

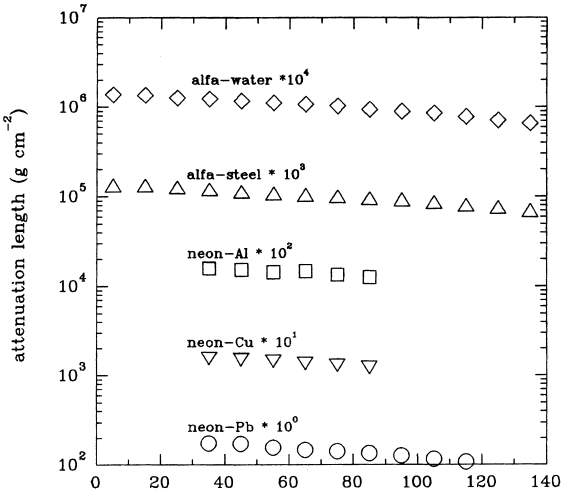

Fig. 8. Attenuation length λ (g cm^{-2}) vs. scoring angle θ for various projectile–target combinations.

the beam is completely stopped in a target. The results of the present work can be compared with those of Ref. [33], where an attenuation length in concrete of 115 g cm^{-2} was found at 0° for 670 MeV/u Ne and Si ions on thick copper targets. The source terms cannot be compared because the present work refers to Ne ions on thin targets.

The recent experimental data by Nakamura et al. [16] should allow to extend the present calculations and build up a more comprehensive data set of source terms and attenuation lengths for ion beam shielding.

References

[1] F. Clapier, Radioactive beam facilities: New thick targets, highlights and challenges, in: Proceedings of the Fourth Specialists' Meeting on Shielding Aspects of Accelerators, Targets and Irradiation Facilities (SATIF4), Knoxville, Tennessee, September 14–15, 1998, in press.
[2] U. Amaldi, B. Larsson, Hadrontherapy in Oncology, Elsevier, Amsterdam, 1994.
[3] M.R. Raju, Heavy Particle Radiotherapy, Academic Press, New York, 1980.
[4] J.R. Castro, in: U. Amaldi, B. Larsson (Eds.), Hadrontherapy and Oncology, Elsevier, Amsterdam, 1994, p. 208.
[5] K. Kawachi et al., in: U. Amaldi, B. Larsson (Eds.), Hadrontherapy and Oncology, Elsevier, Amsterdam, 1994, p. 229.
[6] G. Kraft et al., in: U. Amaldi, B. Larsson (Eds.), Hadrontherapy and Oncology, Elsevier, Amsterdam, 1994, p. 217.
[7] U. Amaldi, M. Silari (Eds.), The TERA Project and the Centre for Oncological Hadrontherapy, Frascati, INFN Publisher, 1994.
[8] D. Campi, M. Silari (Eds.), The TERA Project and the Centre for Oncological Hadrontherapy – Updates and Revisions, Frascati, INFN Publisher, 1994.
[9] S. Agosteo, A. Fassò, A. Ferrari, P.R. Sala, M. Silari, P. Tabarelli de' Fatis, Nucl. Instr. and Meth. B 114 (1996) 70.
[10] K. Shin, K. Miyara, Y. Uwamino, Nucl. Instr. and Meth. A 349 (1994) 506.
[11] K. Shin, K. Miyahara, E. Tanabe, Y. Uwamino, Nucl. Sci. Eng. 120 (1995) 40.
[12] H.R. Schelin et al., Nucl. Sci. Eng. 113 (1993) 184.
[13] R.A. Cecil, B.D. Anderson, A.R. Baldwin, R. Madey, W. Schimmerling, J.W. Kast, D. Ortendahl, Phys. Rev. C 24 (1981) 2013.
[14] R. Madey, J.C. Varga, B.D. Anderson, A.R. Baldwin, R. Cecil, J.W. Watson, G.D. Westfall, in: Proceedings of the Sixth High Energy Ion Study, LBL, University of California, June 28–July 1 1983, p. 317.
[15] R.A. Cecil, B.D. Anderson, A.R. Baldwin, R.A. Madey, Galonsky, P. Miller, L. Young, F.M. Waterman, Phys. Rev. C 21 (1980) 2471.
[16] T. Nakamura, T. Kurosawa, N. Nakao, T. Shibata, Y. Uwamino, A. Fukumura, A systematic experimental study of thick-target neutron yield for high-energy heavy ions, in: Proceedings of the Fourth Specialists' Meeting on Shielding Aspects of Accelerators, Targets and Irradiation Facilities (SATIF4), Knoxville, Tennessee, September 14–15, 1998, in press.

[17] H.W. Bertini, R.T. Santoro, O.W. Hermann, Phys. Rev. C 14 (1976) 590.
[18] T.J.M. Symons et al., Phys. Lett. B 94 (1980) 131.
[19] T.C. Awes, C.K. Gelbe, G. Poggi, B.B. Back, B. Glagola, H. Breuer, V.E. Viola, T.J.M. Symons, Phys. Rev. Lett. 45 (1980) 513.
[20] T.C. Awes, G. Poggi, S. Saini, C.K. Gelbe, R. Legrain, G.D. Westfall, Phys. Lett. B 103 (1981) 417.
[21] T.C. Awes, S. Saini, G. Poggi, C.K. Gelbe, D. Cha, R. Legrain, G.D. Westfall, Phys. Rev. C 25 (1982) 2361.
[22] T. Kato, T. Nakamura, Nucl. Instr. and Meth. A 311 (1992) 548.
[23] K. Shin, K. Miyahara, E. Tanabe, Y. Uwamino, Nucl. Sci. Eng. 120 (1995) 136.
[24] A. Fassò, A. Ferrari, J. Ranft, P.R. Sala, in: Proceedings of the AEN/NEA Specialists' Meeting on Shielding Aspects of Accelerators, Targets and Irradiation Facilities, Arlington (Texas), 28–29 April 1994, NEA/OECD (1995), 287.
[25] A. Fassò, A. Ferrari, J. Ranft, P.R. Sala, G.R. Stevenson, J.M. Zazula, Nucl. Instr. and Meth. A 332 (1993) 459.
[26] A. Fassò, A. Ferrari, J. Ranft, P.R. Sala, G.R. Stevenson, J.M. Zazula, in: Proceedings of the Workshop on Simulating Accelerator Radiation Environment, Santa Fe, 11–15 January 1993. Los Alamos National Laboratory LA-12835-C. Editor: Palounek, A. Los Alamos, New Mexico, (1994) 134.
[27] A. Fassò, A. Ferrari, J. Ranft, P.R. Sala, in: Proceedings of the Fourth International Conference on Calorimetry in High Energy Physics, La Biodola, Italy, 21–26 September 1993. Eds. A. Menzione, A. Scribano, World Scientific, Singapore (1994) 493.
[28] A. Ferrari, P.R. Sala, G. Guaraldi, F. Padoani, Nucl. Instr. and Meth. B 71 (1992) 412.
[29] A. Ferrari, P.R. Sala, in: P. Dragovitsch, S.L. Linn, M. Burbank (Eds.), Proceedings of the MC93 International Conference on Monte Carlo Simulation in High-Energy and Nuclear Physics, Tallahassee, 22–26 February 1993. World Scientific, Singapore (1994) 277.
[30] NCRP Report 51, Radiation Protection Design Guidelines for 0.1–100 MeV Particle Accelerator Facilities (1977).
[31] A.V. Sannikov, E.N. Savitskaya, CERN/TIS-RP/93-14 (1993).
[32] A. Ferrari, M. Pelliccioni, Rad. Prot. Dosim. 51 (1994) 251.
[33] J.B. McCaslin, P.R. LaPlant, A.R. Smith, W.P. Swanson, R.H. Thomas, IEEE Trans. Nucl. Sci. NS-32 (1985) 3104.